



## An Unsteady Hiemenz Stagnation Point Flow of MHD Casson Nanofluid Due to a Superlinear Stretching/Shrinking Sheet with Heat Transfer

Angadi Basetappa Vishalakshi<sup>1,\*</sup>, Ulavathi Shettar Mahabaleshwar<sup>1,\*</sup>, Giulio Lorenzini<sup>2,♣</sup>

<sup>1</sup> Department of Mathematics, Shivagangotri, Davangere University, Davangere, India

<sup>2</sup> Department of Engineering and Architecture, University of Parma, Parco Area delle Scienze 181/A, 43124 Parma, Italy

### ARTICLE INFO

#### Article history:

Received 6 January 2022

Received in revised form 10 April 2022

Accepted 15 April 2022

Available online 19 May 2022

#### Keywords:

Unsteady; stagnation point; nanofluid;  
Casson fluid; Biot number; dual nature

### ABSTRACT

This paper presents the study of an unsteady rear stagnation point flow of an inclined magnetohydrodynamics Casson nanofluid in the attendance of mass transpiration and thermal radiation in energy equation. Graphene nanoparticles are immersed in the flow of a fluid for getting better rate of heat transfer. In this problem is given in nonlinear partial differential equation form and then it is mapped into nonlinear ordinary differential equation form, the resulting equation solved analytically with Biot number and then expressed the solution in closed form incomplete gamma function. The dual nature is also observed in the shrinking sheet case for certain values of parameters. Further, one solution for stretching sheet case. Impact of different parameters, alternates the performance of the entire flow in both stretching and shrinking case, the results can be discussed with the help of graphical representations. These problems arise in engineering field and industrial applications namely extrusion process, metal thinning, glass blowing etc.

## 1. Introduction

Problems with magnetohydrodynamic flow is place a vital part because the effect of magnetic field on the fluid flow is pertinent in numerous industrial cycles viz., preparing magnetic materials, crude oil purification, metal thinning, etc. Pavlov [1] illustrated the impact of magnetic field on fluid flow. Some other results on MHD can be found in the Ref. [2-6]. Investigations on MHD non-Newtonian fluid flow past a superlinear stretching/shrinking sheet also attract many of them because of its various significances in many fields. Kumar *et al.*, [7] and Vinay Kumar *et al.*, [8] and Siddheshwar *et al.*, [9] illustrated on superlinear MHD stretching sheet problems with various physical parameters. On the other hand, some works devoted on unsteady flow situation. Fang and Zhang [10] investigated

\* Corresponding author.

E-mail address: [vishalavishu691@gmail.com](mailto:vishalavishu691@gmail.com)

\* Corresponding author.

E-mail address: [u.s.m@davangereuniversity.ac.in](mailto:u.s.m@davangereuniversity.ac.in)

♣ Corresponding author.

E-mail address: [giulio.lorenzini@unipr.it](mailto:giulio.lorenzini@unipr.it)

<https://doi.org/10.37934/arfmts.95.1.119>

on unsteady boundary layer flows, this technique contains a consistent speed stretching sheet from a space, and the slot is moving at a specific speed contingent on the slot moving boundary.

Recently Mahabaleshwar *et al.*, [11] Benos *et al.*, [12], and Anusha *et al.*, [13] investigated an unsteady flow with mass transpiration and thermal radiation and magnetohydrodynamics to conclude new results. This unsteady flows are different from steady flows; hence one extra term is including in the governing equation of the stretching/shrinking sheet problems. Recent developments in nanotechnology have attract the researchers to study the stretching sheet problems with nanofluids. Nanofluids have unique physical and chemical properties and containing good thermal conductivity. Choi [14] is the pioneer to investigated these type of problems later many researchers worked on stretching sheet problems with nanofluids [15-17]. Casson fluid model is utilized to describe the non-Newtonian fluid flow. Mahabaleshwar *et al.*, [18], Vinay Kumar *et al.*, [19] and Swati *et al.*, [20] conducted a research on Casson fluid flows for both steady and unsteady cases by using various physical parameters. Pramanik [21] investigated on Casson fluid flow past an exponentially porous stretching sheet with heat transfer in the attendance of thermal radiation.

Inspired by above mentioned results the current article is investigation on unsteady flow of a Casson fluid flow over a superlinear stretching/shrinking sheet. In this flow the effective inclined magnetic field is immersed also graphene nanoparticles are added in the fluid flow for getting better thermal efficiency. By using suitable similarity variables PDEs are mapped into ODEs. This equation solved analytically and then expressed the energy equation is in the form of closed form incomplete gamma function. By using different parameters namely Prandtl number, radiation parameter, mass transpiration, Casson fluid parameter, unsteadiness parameter, and Biot number, the result can be analyzed. Dual solution is observed at shrinking sheet case, only one solution is observed at stretching sheet case. FBL and BBL can be defined on the basis of velocity factor of stretching/shrinking parameter. With the help of graphical arrangements, the results can be concluded. Present paper is well argument with Fang and Jing [22] and Mahabaleshwar *et al.*, [23] work.

## 2. Mathematical Analysis

A 2-D Non-Newtonian incompressible rear stagnation-point flow of an inclined MHD Casson fluid is considered in the current investigation. The flow is happened over a stretching/shrinking the sheet with an unsteady free stream velocity  $U_\infty = -\frac{bx}{1-\alpha t}$ , where  $b$  and  $\alpha$  are constants. If  $b > 0$  indicates stretching case and  $b < 0$  indicates shrinking case. The Cartesian coordinates  $(x, y)$  can be arranged as represented in the Figure 1. Graphene nanoparticles are inserted in the fluid to get better thermal efficiency and the nanofluid quantities are represented in the Table 1. External free stream velocity at the wall can be defined by  $U_w = -\lambda U_\infty$ . Here,  $\lambda$  is the unknown constant to be determined, on the basis of value of  $\lambda$  it is indicated that if  $\lambda > 0$ , allows the flow and  $\lambda < 0$  should be restrict the flow. The specific heat flux at wall is defined by  $q_w = -\kappa \frac{\partial T}{\partial y}$  or  $T_w = T_\infty$ .

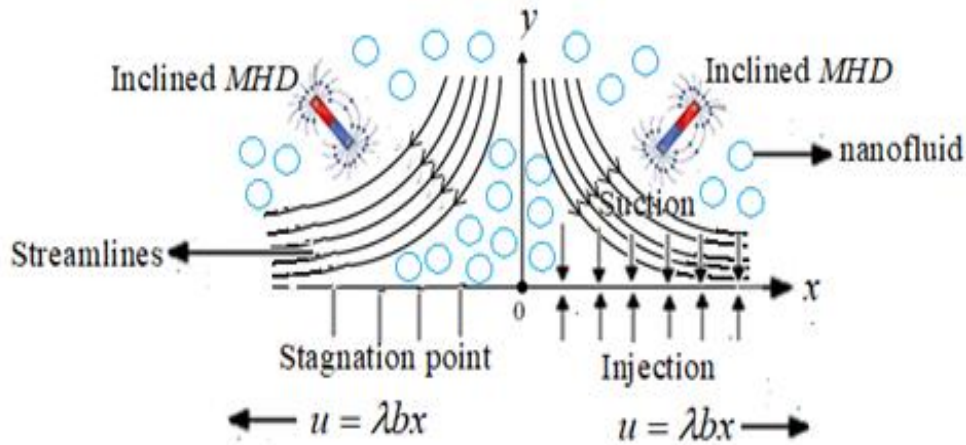


Fig. 1. Schematic diagram of Casson nanofluid flow

The Navier's stokes equation for the present problem can be represented by

$$\frac{\partial u}{\partial x} + \frac{\partial v}{\partial y} = 0, \tag{1}$$

$$\rho_{nf} \left( \frac{\partial u}{\partial t} + u \frac{\partial u}{\partial x} + v \frac{\partial u}{\partial y} \right) = -\frac{\partial P}{\partial x} + \mu_{nf} \left( 1 + \frac{1}{\Lambda} \right) \left( \frac{\partial^2 u}{\partial x^2} + \frac{\partial^2 u}{\partial y^2} \right) + \sigma_{nf} B^2 \sin^2 \xi (U_\infty - u), \tag{2}$$

$$\rho_{nf} \left( \frac{\partial v}{\partial t} + u \frac{\partial v}{\partial x} + v \frac{\partial v}{\partial y} \right) = -\frac{\partial P}{\partial y} + \mu_{nf} \left( 1 + \frac{1}{\Lambda} \right) \left( \frac{\partial^2 v}{\partial x^2} + \frac{\partial^2 v}{\partial y^2} \right), \tag{3}$$

$$(\rho C_p)_{nf} \left( \frac{\partial T}{\partial t} + u \frac{\partial T}{\partial x} + v \frac{\partial T}{\partial y} \right) = \kappa_{nf} \left( \frac{\partial^2 T}{\partial x^2} + \frac{\partial^2 T}{\partial y^2} \right) - \frac{\partial q_r}{\partial y} \tag{4}$$

Boundary conditions utilized with these equations as

$$u = \frac{\lambda bx}{1 - \alpha t}, \quad v = V_w, \quad \text{at } y = 0 \quad u = -\frac{bx}{1 - \alpha t} \quad \text{as } y \rightarrow \infty, \tag{5}$$

$$-\kappa_f \frac{\partial T}{\partial y} = h(T_w - T_\infty) \quad \text{at } y = 0 \quad T \rightarrow T_\infty \quad \text{as } y \rightarrow \infty \tag{6}$$

Here,  $B(x, t)$  denotes the strength of magnetic field applied perpendicular to the surface and it is defined by  $B(x, t) = B_0 / \sqrt{1 - \alpha t}$ . The rest of the parameters mentioned in the above equations can be explained in Nomenclature. By using the factor  $b$  it is easy to classify FBL and BBL. The flow coming from the slot and run along  $+\infty$  is identified as FBL and the stretching from  $+\infty$  and run along the slot is identified as BBL.

**Table 1**  
 Thermophysical properties of graphene and water

Fluids	$C_p (JkgK^{-1})$	$\rho (kgm^{-3})$	$\kappa (WmK^{-1})$	$\sigma (\square m^{-1})$
Water	4179	997.1	0.613	0.05
Graphene	2100	2250	2500	$1 \times 10^7$

Now, define the following similarity transformations to convert PDEs into ODEs.

$$\psi(x, y, t) = x \sqrt{\frac{vb}{1-\alpha t}} f(\eta), \quad \eta = y \sqrt{\frac{b}{v(1-\alpha t)}}, \quad \theta(\eta) = \frac{T - T_\infty}{T_w - T_\infty} \tag{7}$$

By using  $\psi$  and  $\eta$  the transverse and tangential velocities can be defined as

$$u = \frac{\partial \psi}{\partial y} = \frac{bx}{1-\alpha t} f_\eta(\eta), \quad v = -\frac{\partial \psi}{\partial x} = -\sqrt{\frac{vb}{1-\alpha t}} f(\eta) \tag{8}$$

### 2.1 Solution of Pressure

In Eq. (3) it is noticed that it is independent of  $x$  term i.e.  $\frac{\partial P}{\partial y} = F(t, y)$  and where  $G(t, x)$  is the constant of integration. It is calculated by the term  $\frac{\partial P}{\partial x} = \frac{\partial G(t, x)}{\partial x}$ , this term is free from  $y$  term. By using Eq. (2) with  $u = U_\infty$  to get the  $\frac{\partial P}{\partial x}$  value

$$-\frac{1}{\rho} \frac{\partial P}{\partial x} = (1-\beta) \frac{\Gamma_1 b^2 x}{(1-\alpha t)^2}, \tag{9}$$

$y$  – direction pressure term can be obtained as

$$\frac{1}{\rho} (P_0 - P) = \frac{\Gamma_1}{2} (1-\beta) \frac{b^2 x^2}{(1-\alpha t)^2} + \Gamma_1 \int \frac{\partial v}{\partial t} dy + \Gamma_1 \frac{v^2}{2} - \Gamma_2 v \frac{\partial v}{\partial y} \tag{10}$$

Here,  $\beta = b/\alpha$  represents the unsteady parameter, by using this parameter flow is classified into two types namely,  $\beta > 0$  for accelerating flow and  $\beta < 0$  for decelerating flow.  $\beta = 0$  indicates the steady state fluid flow.

### 2.2 Analytical Solution of Momentum and Energy Equation

On applying the similarity transformations and pressure term defined in Eq. (7), (8) and (9) respectively into the Eq. (1) to (4) to get the following ODEs

$$\Gamma_2 \left(1 + \frac{1}{\Lambda}\right) f_{\eta\eta\eta} + \Gamma_1 \left\{ \eta f_{\eta\eta} - f_{\eta}^2 + 1 - \beta \left( f_{\eta} + \frac{1}{2} \eta f_{\eta\eta} + 1 \right) \right\} - \Gamma_3 Q \text{Sin}^2 \xi (1 + f_{\eta}) = 0, \quad (11)$$

$$(\Gamma_5 + R) \theta_{\eta\eta} + \Gamma_4 \text{Pr} \left( f - \frac{\beta \eta}{2} \right) \theta_{\eta} = 0 \quad (12)$$

Boundary conditions related with these equations are reduced into following form

$$f_{\eta}(0) = \lambda, \quad f(0) = V_C, \quad f_{\eta}(\infty) = -1, \quad (13)$$

$$\theta_{\eta}(0) = -Bi(1 - \theta(0)), \quad \theta(\infty) \rightarrow 0. \quad (14)$$

Here,  $Q = \frac{\sigma B_0^2}{\rho b}$  is Chandrasekhar's number,  $\text{Pr} = \frac{(\mu C_p)_f}{\kappa_f}$  is Prandtl number,  $R = \frac{16\sigma^* T_{\infty}^3}{3\kappa_f k^*}$  is the radiation parameter it can be calculated by using Rosseland's approximation, on the basis of this  $q_r$  is modelled as  $q_r = -\frac{4\sigma^*}{3k^*} \frac{\partial T^4}{\partial y}$ , then the term  $T^4$  can be expand by using Taylor's series and ignoring higher order terms to get  $T^4 = -3T_{\infty}^3 + 4T_{\infty}^3 T$ . on substituting these terms into Eq. (4) to get  $\frac{\partial q_r}{\partial y} = -\frac{16\sigma^* T_{\infty}^3}{3k^*} \frac{\partial^2 T}{\partial y^2}$  (see Mahabaleshwar *et al.*, [24,25]), by using this the thermal radiation  $R$  can be calculated. Also, nanofluid quantities  $\varepsilon_1$  to  $\varepsilon_5$  is given by

$$\Gamma_1 = \frac{\rho_{nf}}{\rho_f}, \quad \Gamma_2 = \frac{\mu_{nf}}{\mu_f}, \quad \Gamma_3 = \frac{\sigma_{nf}}{\sigma_f}, \quad \Gamma_4 = \frac{(\rho C_p)_{nf}}{(\rho C_p)_f}, \quad \Gamma_5 = \frac{\kappa_{nf}}{\kappa_f}.$$

In the present analysis the specific value of  $\beta$  value is to be considered, it means to take decelerating flow  $\beta = -2$ . Therefore, the altered equation becomes

$$\Gamma_2 \left(1 + \frac{1}{\Lambda}\right) f_{\eta\eta\eta} + \Gamma_1 \left\{ \eta f_{\eta\eta} - f_{\eta}^2 + 1 + 2 \left( f_{\eta} + \frac{1}{2} \eta f_{\eta\eta} + 1 \right) \right\} - \Gamma_3 Q \text{Sin}^2 \xi (1 + f_{\eta}) = 0, \quad (15)$$

$$(\Gamma_5 + R) \theta_{\eta\eta} + \Gamma_4 \text{Pr} (f + \eta) \theta_{\eta} = 0. \quad (16)$$

In Eq. (15) the term  $\Gamma_2 \left(1 + \frac{1}{\Lambda}\right) f_{\eta\eta\eta} + \Gamma_1 (\eta f_{\eta\eta} - f_{\eta}^2) = 0$ , converted into the results of Hiemenz [26] when  $\Lambda = \infty, \Gamma_1 = \Gamma_2 = 1$ , with imposed boundary condition  $f(0) = f_{\eta}(0) = 0, f_{\eta}(\infty) = 1$ . the 2<sup>nd</sup> term  $\left( f_{\eta} + \frac{1}{2} \eta f_{\eta\eta} + 1 \right)$  indicates the unsteady effect, and  $Q \text{Sin}^2 \xi (1 + f_{\eta})$  indicates the Lorentz force.

Introduce another variable  $F(\eta) = f(\eta) + \eta$  for the purpose of solving the momentum equation. Then the Eq. (15) is transformed as

$$\Gamma_2 \left( 1 + \frac{1}{\Lambda} \right) F_{\eta\eta\eta} + \Gamma_1 (FF_{\eta\eta} + 4F_\eta - F_\eta^2) - \Gamma_3 Q \text{Sin}^2 \xi F_\eta = 0, \quad (17)$$

the dimensionless boundary conditions Eq. (13) also transformed as

$$F(0) = V_C, \quad F_\eta(0) = \lambda + 1, \quad F_\eta(\infty) = 0. \quad (18)$$

Solution of Eq. (17) can be assumed as

$$F = m + n \exp(-\gamma\eta) \quad \gamma > 0 \quad (19)$$

By using Eq. (18) and (19) into Eq. (17) to yield following results

$$r\gamma^2 - \Gamma_1 m\gamma + (4\Gamma_1 - \Gamma_3 Q \text{Sin}^2 \xi) = 0, \quad (20)$$

$$n = -\frac{\lambda + 1}{\gamma}, \quad m = V_C + \frac{\lambda + 1}{\gamma}, \quad (21)$$

$$m + n = V_C \quad (22)$$

The solution of Eq. (20) is given by

$$\gamma = \frac{\Gamma_1 V_C \pm \sqrt{(\Gamma_1 V_C)^2 + 4d(\Gamma_1 \lambda + \Gamma_3 Q \text{Sin}^2(\xi) - 3\Gamma_1)}}{2d} \quad (23)$$

where  $d = \Gamma_2 \left( 1 + \frac{1}{\Lambda} \right)$

For a physically feasible solution,  $\gamma$  must be greater than zero, and Eq. (20) containing real solutions also it is satisfy  $(\Gamma_1 V_C)^2 + 4d(\Gamma_1 \lambda + \Gamma_3 Q \text{Sin}^2 \xi - 3\Gamma_1) \geq 0$ . Negative solution of Eq. (20) it mathematically possible but not physically available. For mass suction there exist two solutions and for mass injection there exist only one solution (see Ref. [22] and [23]).

Then the solution of the general problem of Eq. (11) is given by

$$f(\eta) = -\eta + V_C + \frac{\lambda + 1}{\gamma} (1 - \exp(-\gamma\eta)), \quad (24)$$

Tangential velocity becomes

$$f_\eta(\eta) = -1 + (\lambda + 1) \exp(-\gamma\eta) \quad (25)$$

where,

$$\gamma = \frac{\Gamma_1 V_c + \sqrt{(\Gamma_1 V_c)^2 + 4d(\Gamma_1 \lambda + \Gamma_3 Q \sin^2 \xi - 3\Gamma_1)}}{2d}, \quad (26)$$

for upper branch solution

$$\gamma = \frac{\Gamma_1 V_c - \sqrt{(\Gamma_1 V_c)^2 + 4d(\Gamma_1 \lambda + \Gamma_3 Q \sin^2 \xi - 3\Gamma_1)}}{2d}, \quad (27)$$

for lower branch solution.

Now, we introduce new variable called  $\varepsilon$  to find the analytical solution of temperature equation and it is defined by

$$\varepsilon = (1 + \lambda) \frac{\text{Pr}}{\gamma^2} \exp(-\gamma \eta) \quad (28)$$

Substituting this new variable into Eq. (16) to get the result in the following form

$$(\Gamma_5 + R) \varepsilon \frac{\partial^2 \theta}{\partial \varepsilon^2} + \left( (\Gamma_5 + R) - \frac{\Gamma_4}{\Gamma_1} \text{Pr} \left( d + \frac{4\Gamma_1 + \Gamma_3 Q \sin^2(\tau)}{\gamma^2} \right) + \Gamma_4 \varepsilon \right) \frac{\partial \theta}{\partial \varepsilon} = 0, \quad (29)$$

the boundary condition associated with this temperature equation also reduces to

$$(\lambda + 1) \frac{\text{Pr}}{\gamma} \theta_\eta \left( (\lambda + 1) \frac{\text{Pr}}{\gamma^2} \right) = -Bi \left( 1 - \theta \left( (\lambda + 1) \frac{\text{Pr}}{\gamma^2} \right) \right), \quad \theta(0) \rightarrow 0 \quad (30)$$

Apply the Frobenius method to deduce the power series solution of Eq. (29), for this consider

$$\theta(\varepsilon) = \sum_{r=0}^{\infty} C_r \varepsilon^{k+r} \quad (C_0 \neq 0) \quad (31)$$

Derivatives of above equation with respect to  $\varepsilon$  is given by

$$\begin{aligned} \frac{\partial \theta}{\partial \varepsilon} &= \sum_{r=0}^{\infty} (k+r) C_r \varepsilon^{k+r-1}, \\ \frac{\partial^2 \theta}{\partial \varepsilon^2} &= \sum_{r=0}^{\infty} (k+r)(k+r-1) C_r \varepsilon^{k+r-2} \end{aligned} \quad (32)$$

By importing Eq. (32) into Eq. (30) to get the following values of  $k$  and recurrence relation respectively.

$$k = 0, \quad k = 1 - \frac{B}{A},$$

where,

$$A = (\Gamma_5 + R), \quad \text{and} \quad B = (\Gamma_5 + R) - \frac{\Gamma_4}{\Gamma_1} \text{Pr} \left( d + \frac{4\Gamma_1 + \Gamma_3 Q \text{Sin}^2(\tau)}{\gamma^2} \right). \quad (33)$$

$$C_r = - \frac{\Gamma_4 (k + r - 1)}{(k + r)(A(k + r - 1) + B)} C_{r-1} \quad (34)$$

with the help of this recurrence relation and the values of  $k$  the solution of Eq. (29) is simplified as

$$\theta(\varepsilon) = C_1 C_0 + C_2 C_0 \left( 1 - \frac{B}{A} \right) (-\Gamma_4)^{-\left(1 - \frac{B}{A}\right)} \left( \Gamma \left( 1 - \frac{B}{A}, 0 \right) - \Gamma \left( 1 - \frac{B}{A}, -\varepsilon \Gamma_4 \right) \right) \quad (35)$$

By using boundary conditions defined in Eq.(30) to get the value of  $C_1$  and  $C_2$  as follows

$$C_1 = 0,$$

$$C_2 = \frac{Bi}{c_0 \left( 1 - \frac{B}{A} \right) (-\Gamma_4)^{\frac{B}{A} - 1}} \left\{ \gamma \left( -(\lambda + 1) \Gamma_4 \frac{\text{Pr}}{\gamma^2} \right)^{1 - \frac{B}{A}} \exp \left( (\lambda + 1) \Gamma_4 \frac{\text{Pr}}{\gamma^2} \right) + \right. \quad (36)$$

$$\left. Bi \Gamma \left( 1 - \frac{B}{A}, 0 \right) - Bi \Gamma \left( 1 - \frac{B}{A}, -(\lambda + 1) \Gamma_4 \frac{\text{Pr}}{\gamma^2} \right) \right\}^{-1}.$$

Substituting  $C_1$  and  $C_2$  values in Eq. (35) to yield the result in terms of  $\eta$  is given by

$$\theta(\eta) = \frac{Bi \Gamma \left( 1 - \frac{B}{A}, 0 \right) - Bi \Gamma \left( 1 - \frac{B}{A}, -(\lambda + 1) \Gamma_4 \frac{\text{Pr}}{\gamma^2} e^{-\eta} \right)}{\left\{ \gamma \left( -(\lambda + 1) \Gamma_4 \frac{\text{Pr}}{\gamma^2} \right)^{1 - \frac{B}{A}} \exp \left( (\lambda + 1) \Gamma_4 \frac{\text{Pr}}{\gamma^2} \right) + Bi \Gamma \left( 1 - \frac{B}{A}, 0 \right) - Bi \Gamma \left( 1 - \frac{B}{A}, -(\lambda + 1) \Gamma_4 \frac{\text{Pr}}{\gamma^2} \right) \right\}} \quad (37)$$

where,  $\Gamma$  represents the incomplete gamma function. Further we discuss the discussion of result with the help of graphical representation as follows.

### 3. Results and discussion

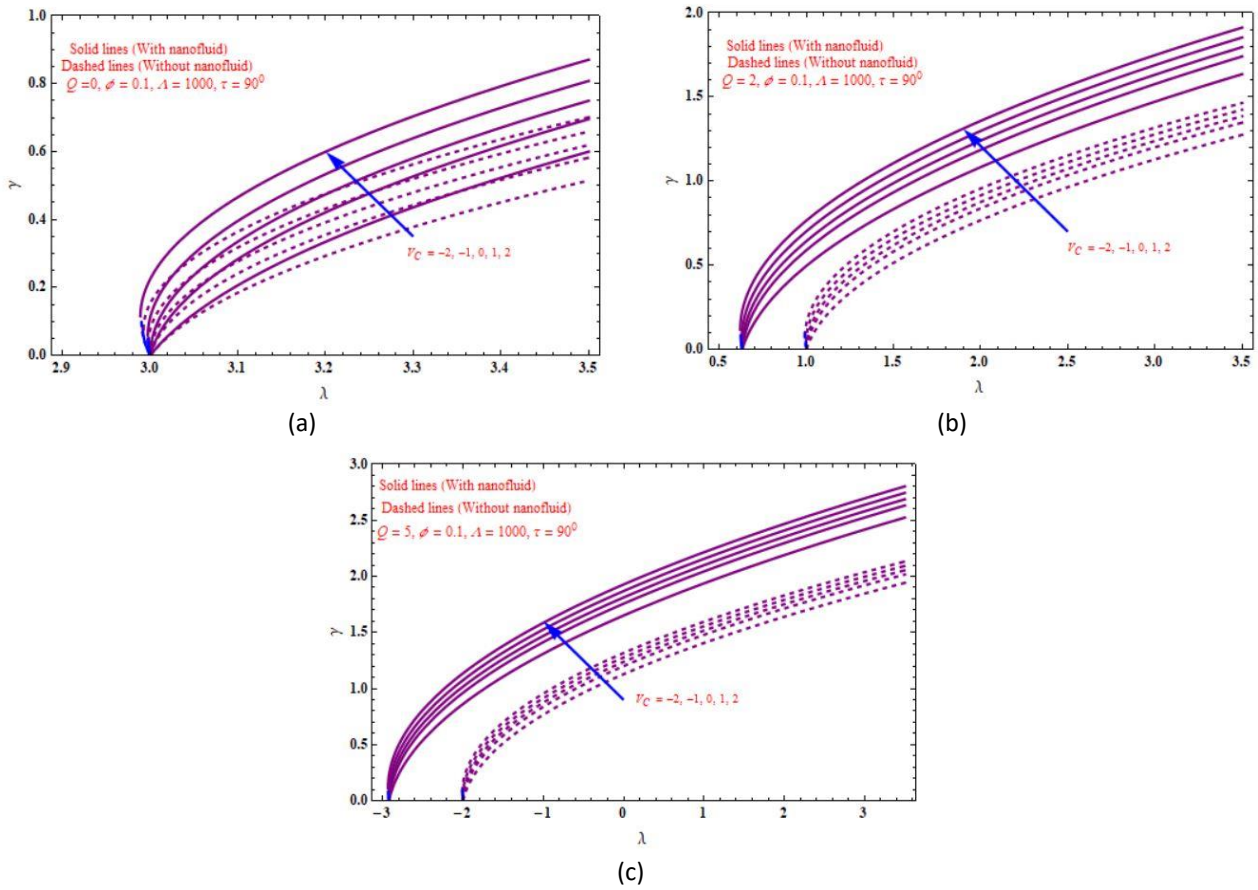
An unsteady laminar flow of a MHD Casson nanofluid flow in the attendance with mass transpiration and thermal radiation is considered in the present analytical problem. Graphene nanoparticles are inserted into the fluid to enhance the thermal conductivity of the fluid. The analytical results can be obtained after converting PDEs to ODEs via similarity transformations. Momentum equation is solved analytically to yield the solution domain. Then this domain used in

energy equation and verified exactly and it is expressed in the form of incomplete gamma function. The solid volume fraction of Graphene nanofluid is utilized in the throughout the problem. Physical scenario can be achieved with the help of different controlling parameters namely, mass transpiration, thermal radiation, Biot number, inclined angle, and solid volume fraction and so on.

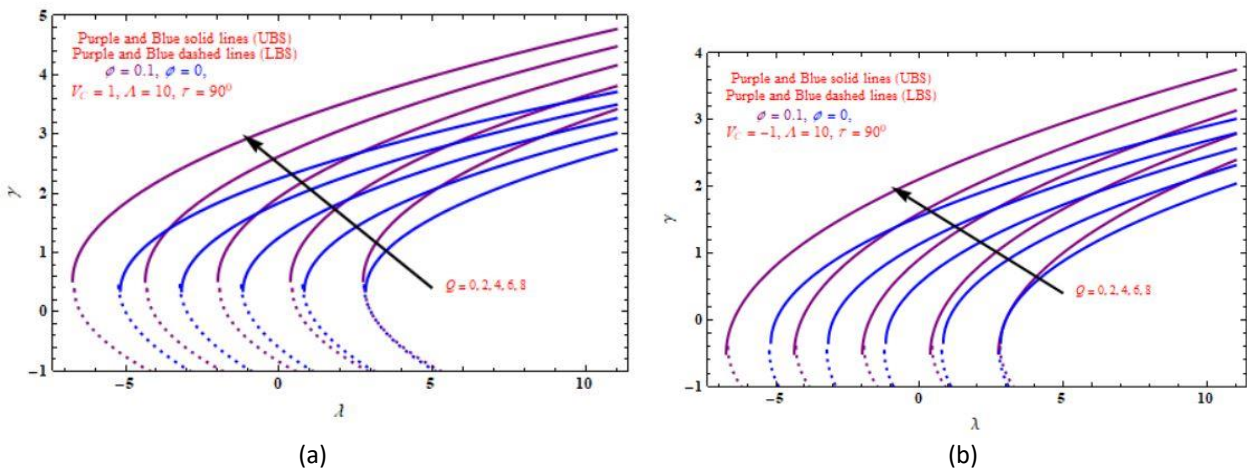
Figure 2(a)-(c) indicates the impact of  $\gamma$  on  $V_C$  as a function of  $\lambda$  for  $Q=0$ ,  $Q=2$  and  $Q=5$ , respectively. As discussed in the above mathematical analysis part at Eq. (23) here it is observed that the dual nature behavior, If  $\gamma > 0$ , it indicates upper branch solution and if  $\gamma < 0$  it indicates lower branch of solution. Upper and lower branch of solutions respectively denoted by solid lines and dashed lines in the figure. In Figure 2(a)-(c) it is clearly seen that  $V_C$  increases the  $\gamma$  value with reduces the values of  $\lambda$ . The dual nature behavior depending on the values of  $Q$  and  $\lambda$ . If the values of  $Q=0$  increases the distance between the lower and upper branch of solution increases and the thickness of the boundary layer flow decreases. These graphs also exhibit the suction injection behavior, if  $V_C = 0$  indicates no permeability,  $V_C > 0$  indicates suction case and  $V_C < 0$  indicates injection case.

Figure 3(a)-(c) portrays the impact of  $\gamma$  on  $\lambda$  for various values of  $Q$  for  $V_C = 0$  (No Permeability)  $V_C > 0$  ( suction) and  $V_C < 0$  ( injection) respectively. In this case also it is seen that  $\gamma$  increases with increase the values of  $Q$  with decreases of  $\lambda$ . Upper solution is observed at solid lines and lower solution branch is indicated at dashed lines. Also, it is observed that the boundary layer flow move towards positive x axis if the value of  $V_C$  increases. Figure 3(a): Impact of  $\gamma$  on  $\lambda$  for different choices of  $Q$  at injection case i.e.  $V_C < 0$ .

Figure 4(a) and (b) indicates the impact of tangential velocity  $f_\eta(\eta)$  on  $\eta$  for various choices of  $V_C$  at the values  $Q=0, \lambda=1$ , and  $Q=1, \lambda=0.1$  respectively. Purple solid lines represent the upper branch solution and blue solid lines indicates the lower branch solution.  $f_\eta(\eta)$  increases with increase the values of  $V_C$  whereas the value of  $V_C$  decreases the  $f_\eta(\eta)$  in upper branch case. It is also seen that distance between upper and lower branch of solution decrease with increases the values of  $Q$ . Figure 4(c) and (d) indicates the impact of  $f_\eta(\eta)$  on  $\eta$  for various choices of  $V_C$  in the presence and absence of nanoparticles. Purple solid lines represents the presence of nanoparticles and the blue dashed lines represents the absence of nanoparticles, in this case it is also observed that thickness of the boundary layer flow is decreases with the increases the values of  $Q$ . Figure 5(a) and (b) indicates the impact of  $f_\eta(\eta)$  on  $\eta$  for various values of  $Q$ , here also it is seen that the same effect as mentioned in Figure 4(a) and (b) i.e.  $f_\eta(\eta)$  more for more values of  $Q$  in the lower branch case and it is reversed in the case of upper branch, and the thickness is larger for large values of  $\lambda$ .



**Fig. 2.** (a) Impact of  $\gamma$  on  $\lambda$  for various values of  $V_C$  at  $Q=0$  (b) Effect of  $\gamma$  on  $\lambda$  for various values of  $V_C$  in the attendance of  $Q=2$  (c) Plot of  $\gamma$  versus  $\lambda$  for various values of  $V_C$  at  $Q=5$



**Fig. 3.** (a) Effect of  $\gamma$  on  $\lambda$  for different choices of  $Q$  at suction case i.e.  $V_C > 0$  (b) Impact of  $\gamma$  on  $\lambda$  for different choices of  $Q$  at injection case i.e.  $V_C < 0$

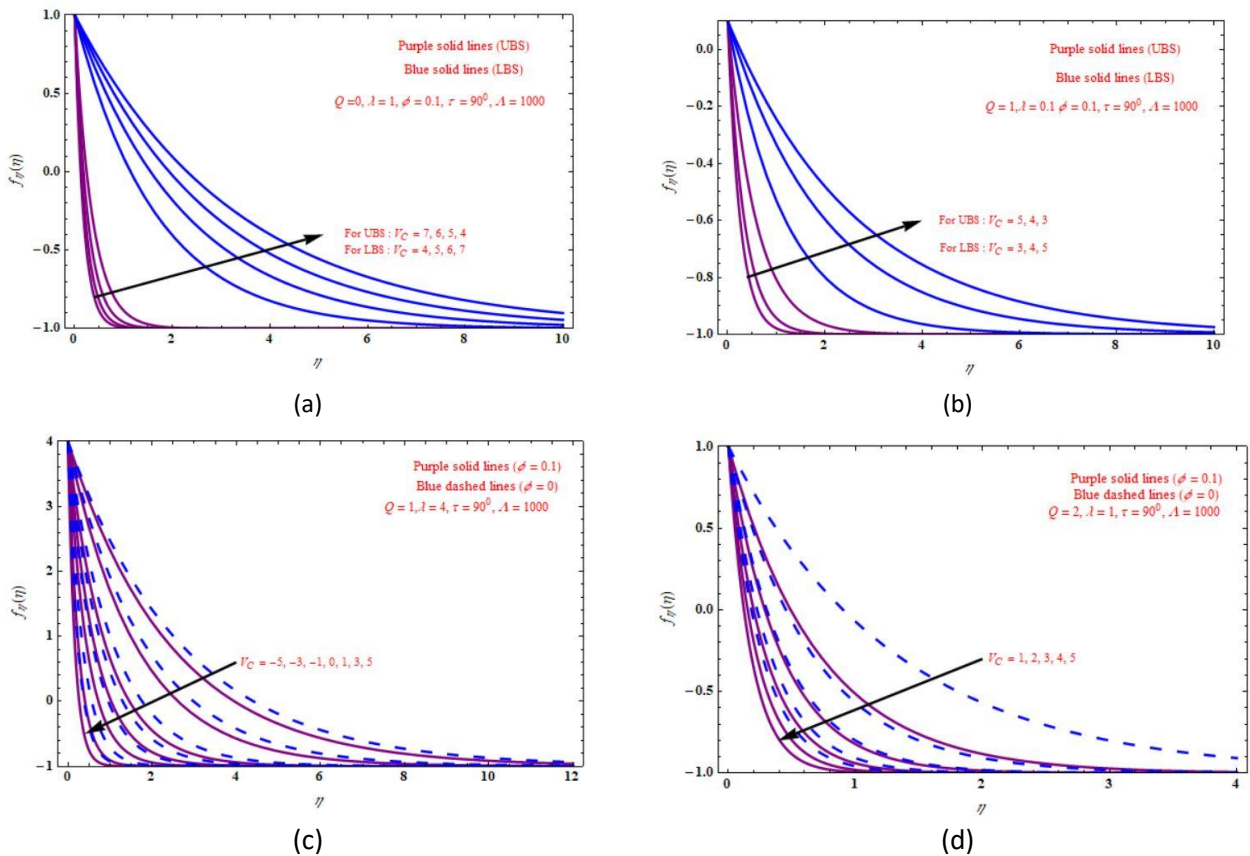


**Fig. 4.** (a) Impact of  $f_{\eta}(\eta)$  on  $\eta$  for upper and lower branch solution at  $Q = 0$  (b) Impact of  $f_{\eta}(\eta)$  on  $\eta$  for upper and lower branch of solution at  $Q = 1$  (c) Plots of  $f_{\eta}(\eta)$  verses  $\eta$  at  $Q = 1$  (d) Plots of  $f_{\eta}(\eta)$  verses  $\eta$  at  $Q = 2$

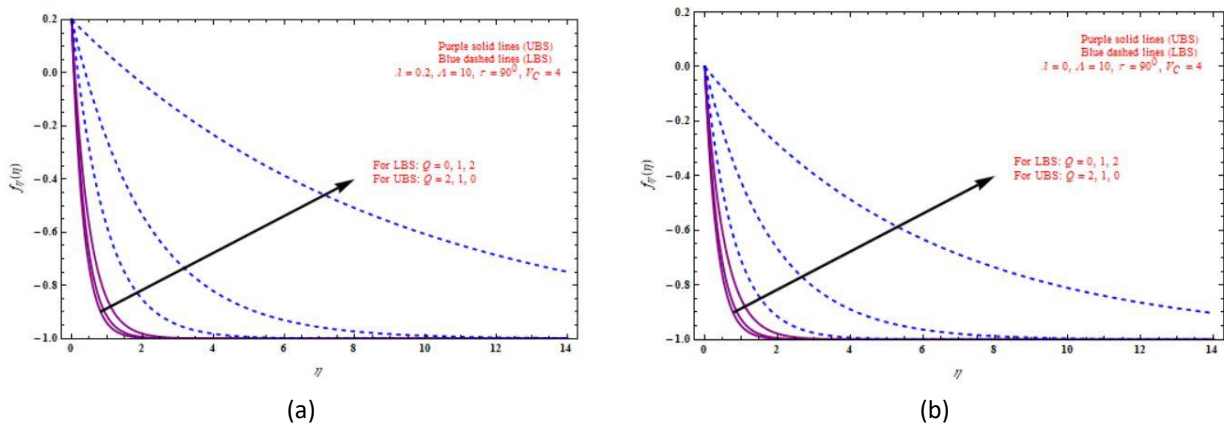


**Fig. 5.** (a) Plots of  $f_{\eta}(\eta)$  verses  $\eta$  at  $\lambda = 0.2$  (b) Plots of  $f_{\eta}(\eta)$  verses  $\eta$  at  $\lambda = 0$

Figure 6(a)-(c) and Figure 7(a)-(c) indicates the impact of  $f_{\eta}(\eta)$  on  $\eta$  for various choices of  $\Lambda$  and  $\phi$  for the cases of no permeability, suction, and injection cases respectively. For these figures Purple solid lines indicates the presence of nanofluid and the blue dashed lines represents the absence of nanofluids. In Figure 6(a)-(c) it is seen that the thickness of boundary value decreases with increase of  $\Lambda$  and it is moving towards  $x$  axis. The similar effect is observed at Figure 7(a)-(c), i.e.

$f_\eta(\eta)$  decreases with increases the values of  $\phi$ , and the thickness of the layer decreases with increases the values of  $V_C$ .

The impact of  $\theta(\eta)$  on  $\eta$  for different choices of  $V_C, Q, \Lambda, Bi$  and  $\phi$  respectively plotted at Figure 8(a)-(e). Purple solid lines indicates the attendance of nanoparticles and blue dashed lines represents the absence of nanoparticles. In all the cases  $\theta(\eta)$  increases with increase of  $V_C, Q, \Lambda, Bi$  and  $\phi$ , and the boundary value thickness moving outwards from the  $x$  axis.

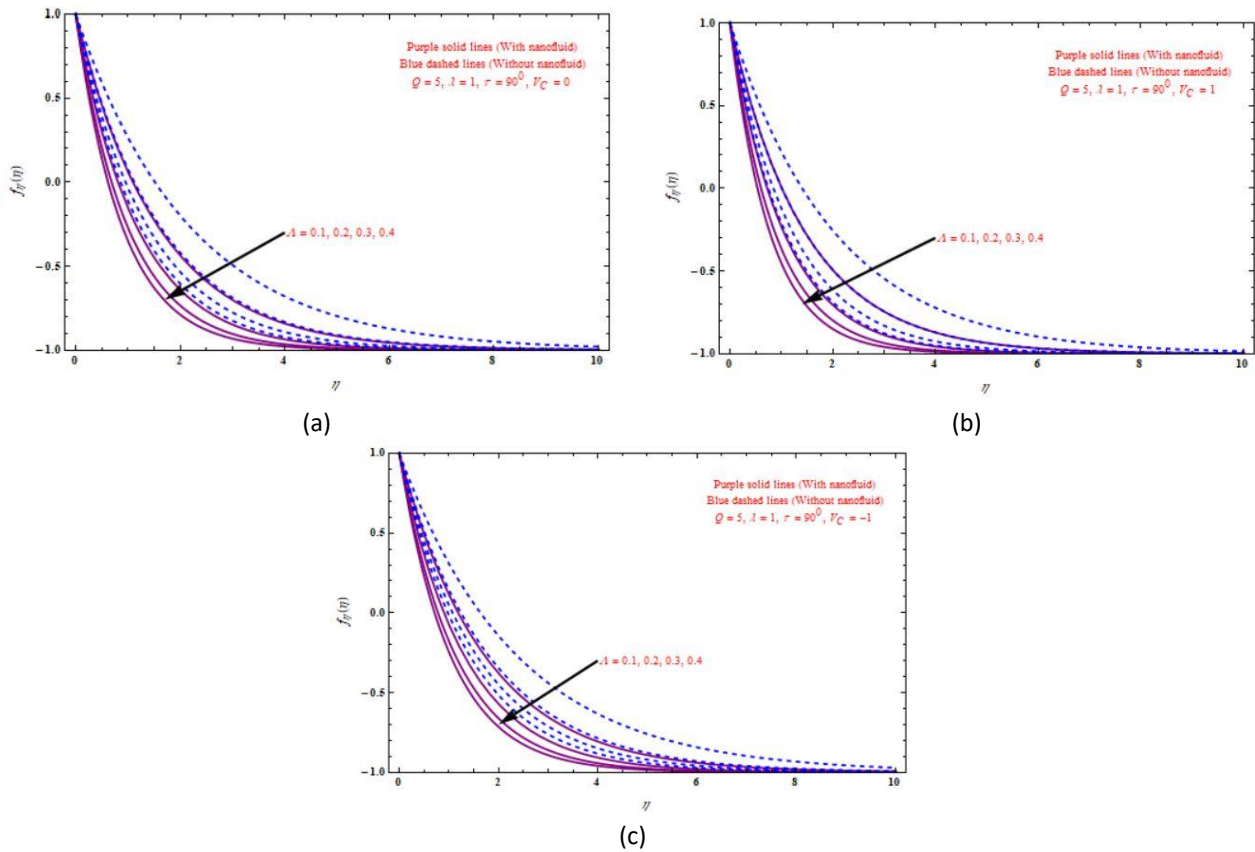


**Fig. 6.** (a) Plots of  $f_n(\eta)$  versus  $\eta$  for different choices of  $\Lambda$  at  $V_C = 0$  (b) Plots of  $f_n(\eta)$  versus  $\eta$  for various choices of  $\Lambda$  for suction case ( $V_C > 0$ ) (c) Plots of  $f_n(\eta)$  versus  $\eta$  for various choices of  $\Lambda$  for injection case ( $V_C < 0$ )

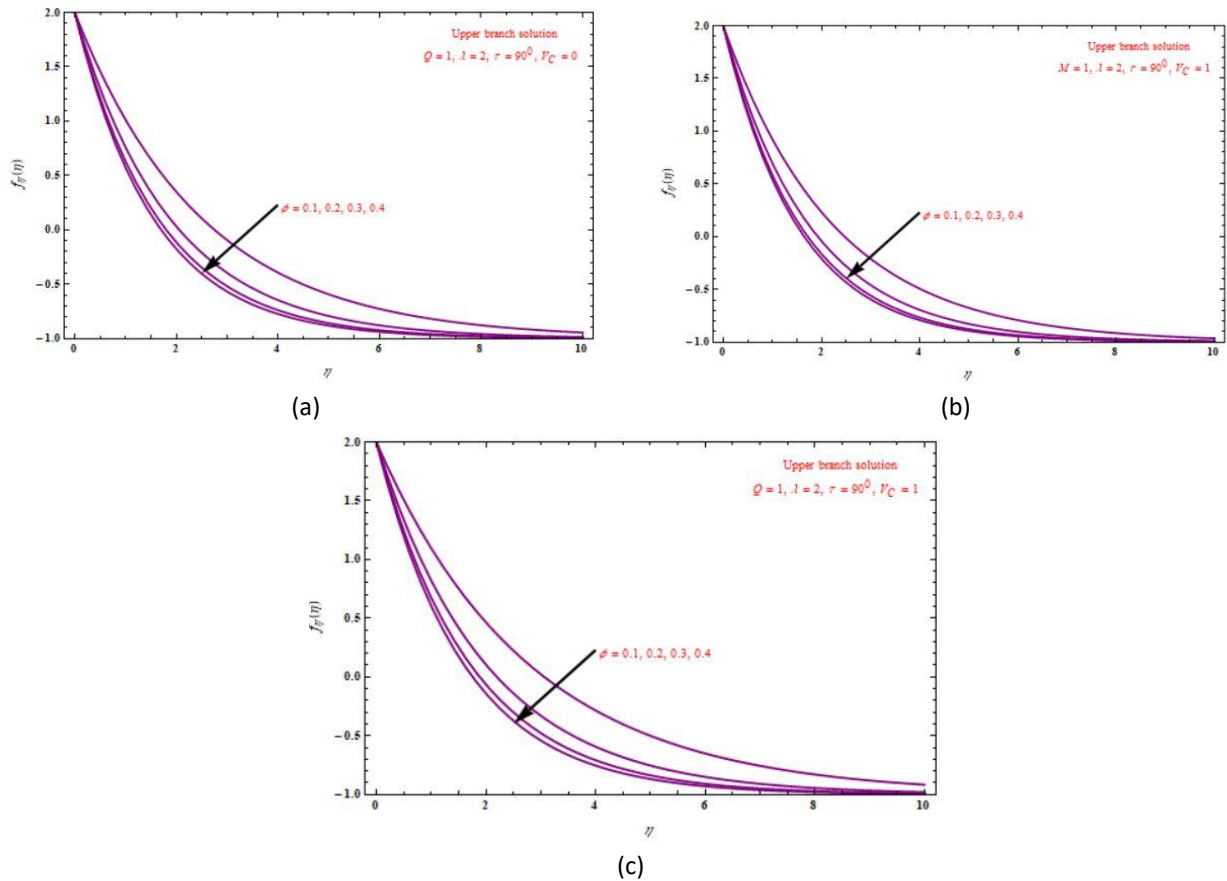


**Fig. 7.** (a) Plots of  $f''_n(\eta)$  versus  $\eta$  for various choices of  $\phi$  at  $V_C = 0$  (b) Plots of  $f''_n(\eta)$  versus  $\eta$  for various choices of  $\phi$  for suction case ( $V_C > 0$ ) (c) Plots of  $f''_n(\eta)$  versus  $\eta$  for various choices of  $\phi$  for injection case ( $V_C < 0$ )

Figure 9(a) and (b) depicts the pattern of streamline flows for suction and injection cases respectively. In both the cases we clearly observe the difference between streamline flows, i.e. different flow patterns are observed at suction and injection cases. Both graphs are plotted for upper branch case also these graphs can be plotted by using stream function defined in Eq. (7). Applied inclined magnetic field causes the significant free flow this results the flattening of the velocity boundary. Figure 10(a) and (b) and Figure 11(a) and (b) represents the effect of tangential and transverse velocities for both suction and injection cases respectively. It can be seen two branches namely, upper branch solution and lower branch solution.

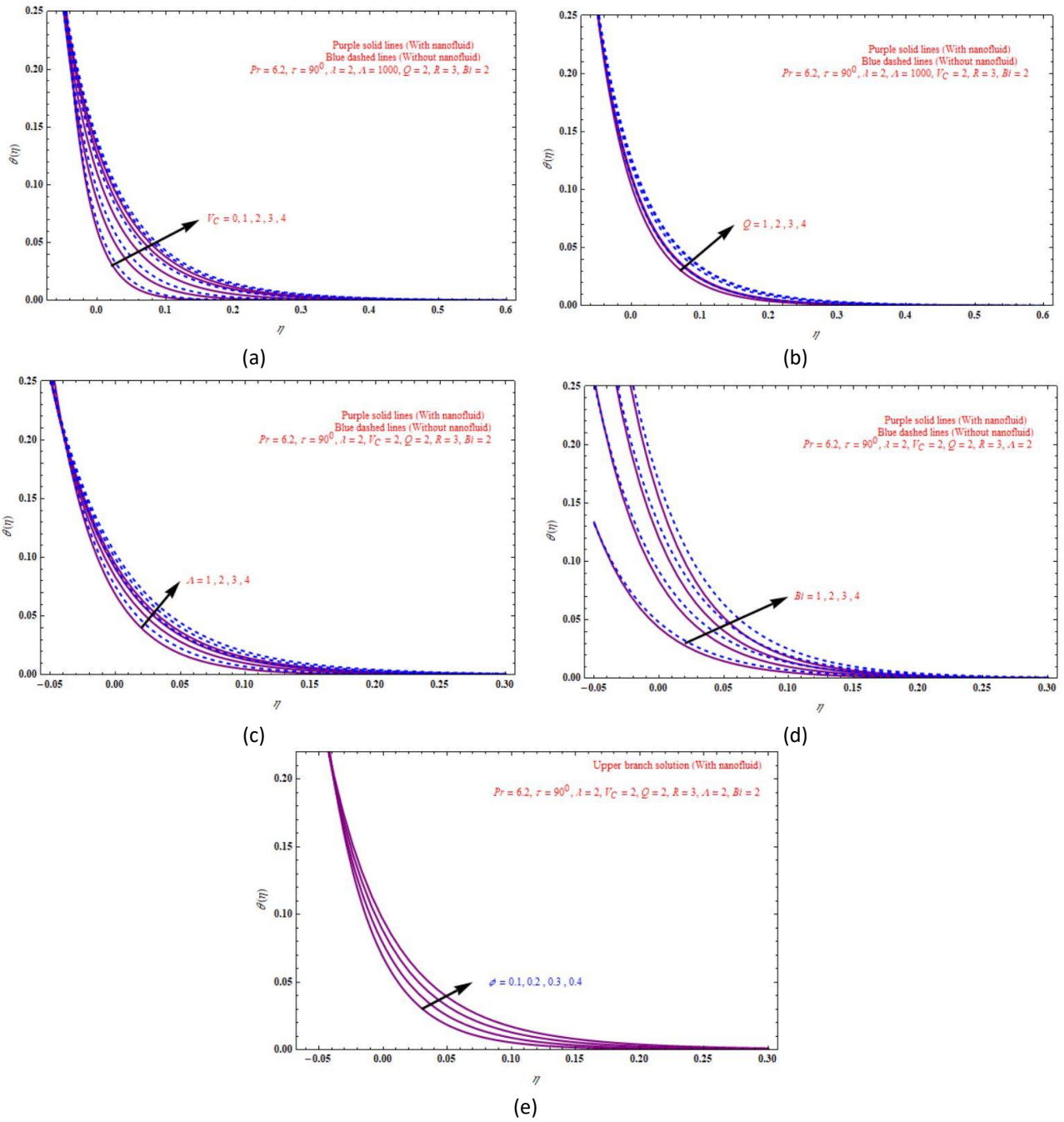
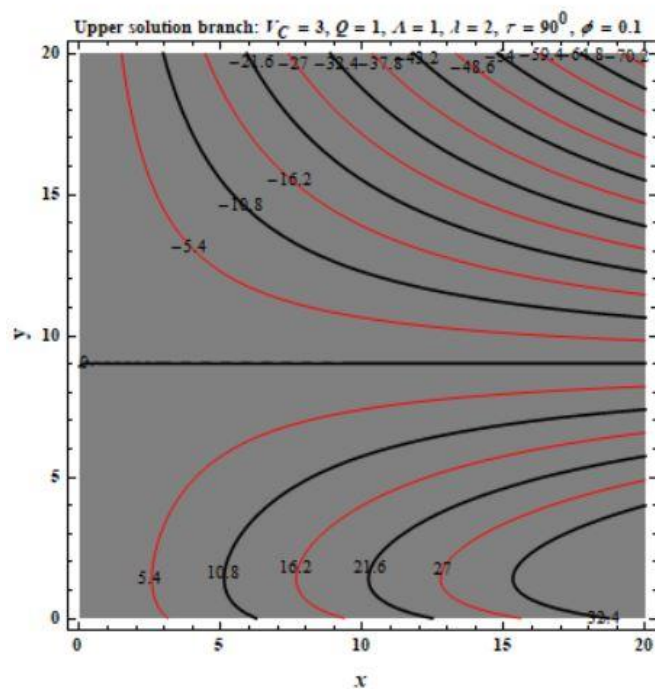
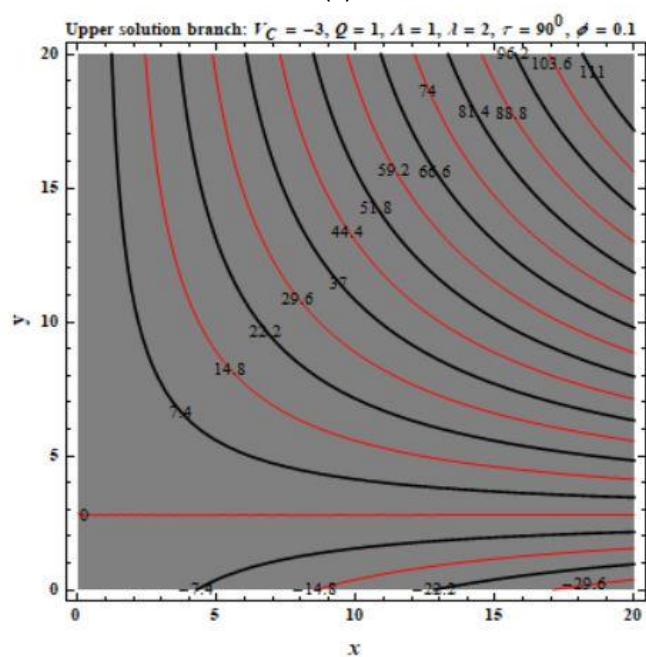


**Fig. 8.** (a) Impact of  $\theta(\eta)$  on  $\eta$  for different choices of  $V_c$  (b) Plots of  $\theta(\eta)$  on  $\eta$  for different choices of  $Q$  (c) Effect of  $\theta(\eta)$  on  $\eta$  for different choices of  $\Lambda$  (d) Plots of  $\theta(\eta)$  versus  $\eta$  for different choices of  $Bi$  (e) Plots of  $\theta(\eta)$  versus  $\eta$  for different choices of  $\phi$

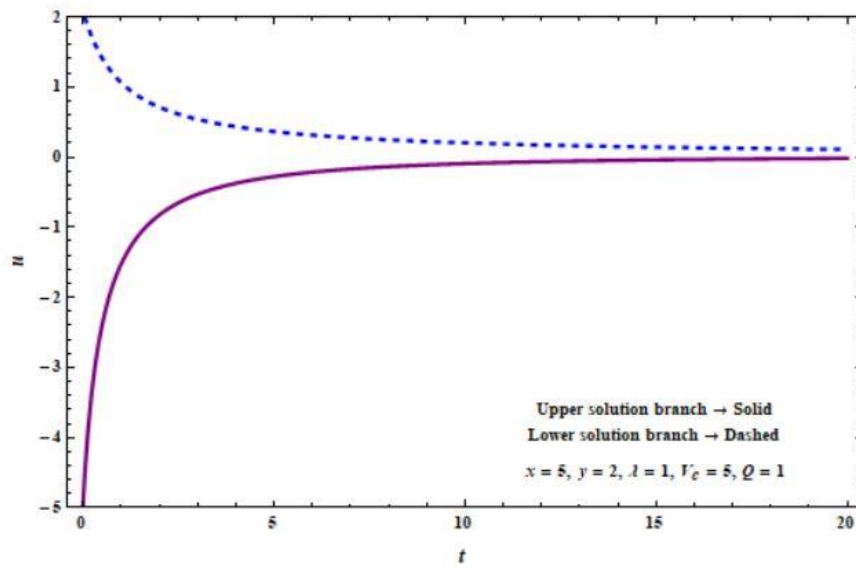


(a)

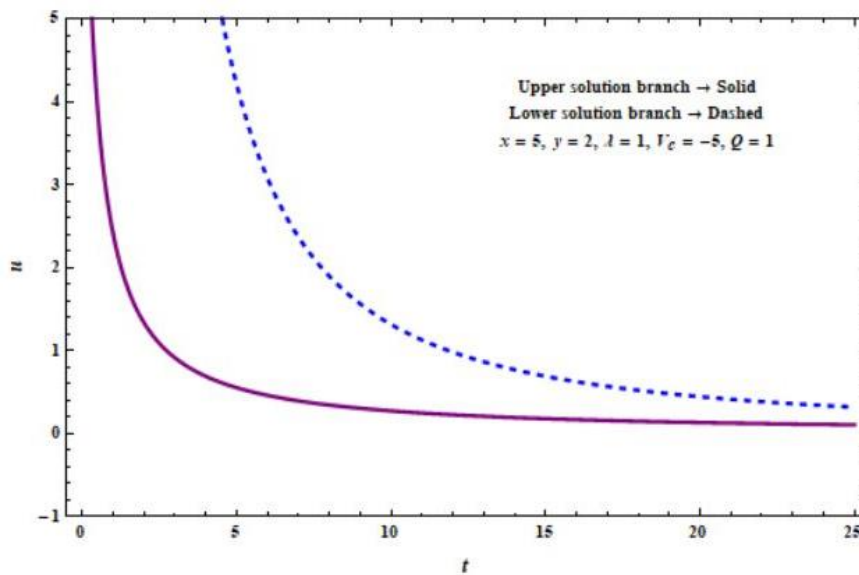


(b)

**Fig. 9.** (a) Contour plots of stream function for suction case ( $V_C > 0$ ) (b) Contour plots of stream function for injection case ( $V_C < 0$ )

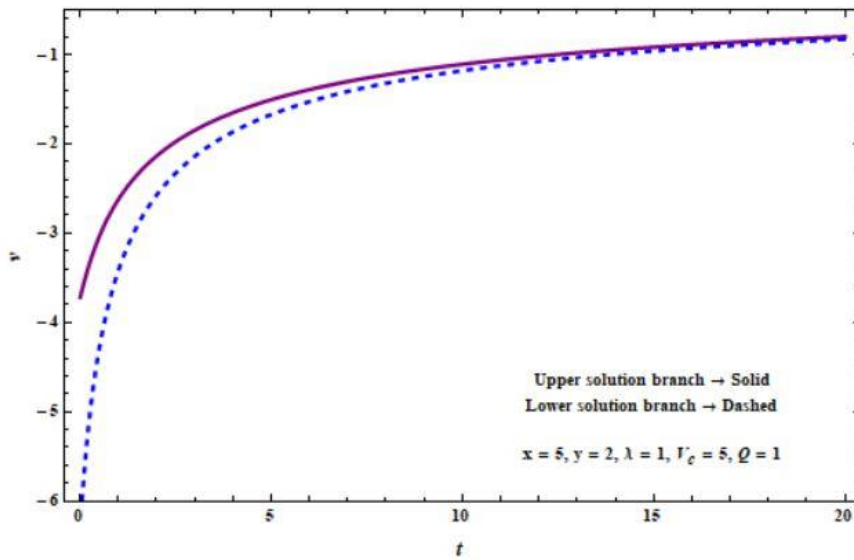


(a)

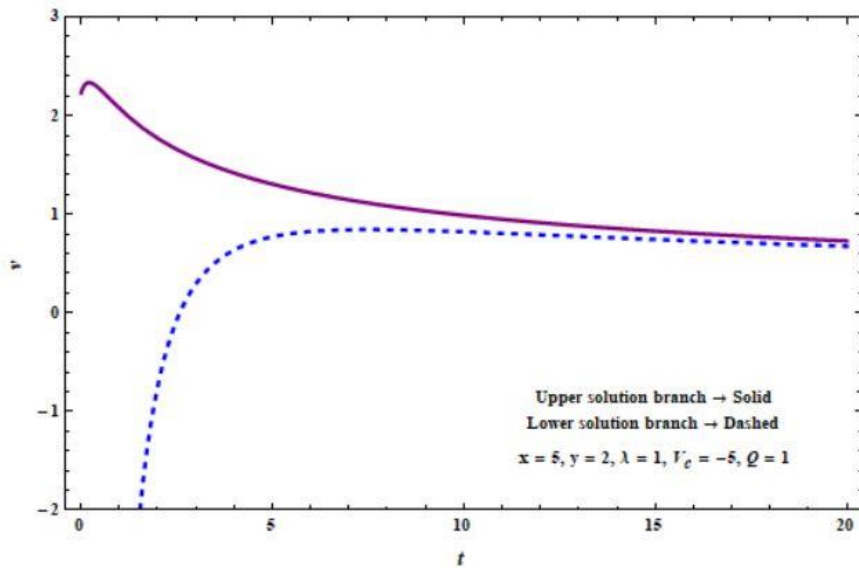


(b)

**Fig. 10.** (a) Tangential velocity components for suction case ( $V_c > 0$ ) (b) Tangential velocity components for injection case ( $V_c < 0$ )



(a)



(b)

**Fig. 11.** (a) Transverse velocity components for suction case ( $V_C > 0$ ) (b) Transverse velocity components for injection case ( $V_C < 0$ )

#### 4. Concluding Remarks

An unsteady rear stagnation point flow of a Casson nanofluid flow past a superlinear stretching/shrinking sheet in the attendance of mass transpiration and radiation is considered to illustrate the new results. The governing PDEs are converted into ODEs via similarity variables and then it is solved analytically and express in terms of incomplete gamma function. The new results can be deduced by using graphical representations.

- i. Dual nature behavior is observed for solution domain
- ii. Value of  $V_C$  increases the  $\gamma$  value with decreases the values of  $\lambda$
- iii.  $\gamma$  is more for more values of  $Q$ .

- iv.  $f_{\eta}(\eta)$  increases with increases of  $V_C$  and  $Q$  for lower branch solution and reduces for upper branch solution.
- v.  $f_{\eta}(\eta)$  decreases for  $\Lambda$ , and  $\phi$ .
- vi.  $\theta(\eta)$  increases with increases of  $V_C$ ,  $Q$ ,  $\Lambda$ ,  $Bi$ , and  $\phi$  values.

## References

- [1] Pavlov, K. B. "Magnetohydrodynamic flow of an incompressible viscous fluid caused by deformation of a plane surface." *Magnitnaya Gidrodinamika* 4, no. 1 (1974): 146-147.
- [2] Andersson, H. I. "An exact solution of the Navier-Stokes equations for magnetohydrodynamic flow." *Acta Mechanica* 113, no. 1 (1995): 241-244. <https://doi.org/10.1007/BF01212646>
- [3] Kumaran, V., A. K. Banerjee, A. Vanav Kumar, and K. Vajravelu. "MHD flow past a stretching permeable sheet." *Applied mathematics and computation* 210, no. 1 (2009): 26-32. <https://doi.org/10.1016/j.amc.2008.10.025>
- [4] Siddheshwar, P. G., and U. S. Mahabaleswar. "Effects of radiation and heat source on MHD flow of a viscoelastic liquid and heat transfer over a stretching sheet." *International Journal of Non-Linear Mechanics* 40, no. 6 (2005): 807-820. <https://doi.org/10.1016/j.ijnonlinmec.2004.04.006>
- [5] Mahabaleswar, U. S., I. E. Sarris, Antony A. Hill, Giulio Lorenzini, and Ioan Pop. "An MHD couple stress fluid due to a perforated sheet undergoing linear stretching with heat transfer." *International Journal of Heat and Mass Transfer* 105 (2017): 157-167. <https://doi.org/10.1016/j.ijheatmasstransfer.2016.09.040>
- [6] Mahabaleswar, U. S., T. Anusha, P. H. Sakanaka, and Suvanjan Bhattacharyya. "Impact of inclined Lorentz force and Schmidt number on chemically reactive Newtonian fluid flow on a stretchable surface when Stefan blowing and thermal radiation are significant." *Arabian Journal for Science and Engineering* 46, no. 12 (2021): 12427-12443. <https://doi.org/10.1007/s13369-021-05976-y>
- [7] Kumar, PN Vinay, U. S. Mahabaleswar, P. H. Sakanaka, and G. Lorenzini. "An MHD effect on a Newtonian fluid flow due to a superlinear stretching sheet." *Journal of Engineering Thermophysics* 27, no. 4 (2018): 501-506. <https://doi.org/10.1134/S1810232818040112>
- [8] Kumar, PN Vinay, U. S. Mahabaleswar, K. R. Nagaraju, Mohaddeseh Mousavi Nezhad, and A. Daneshkhah. "Mass transpiration in magneto-hydrodynamic boundary layer flow over a superlinear stretching sheet embedded in porous medium with slip." *Journal of Porous Media* 22, no. 8 (2019). <https://doi.org/10.1615/JPorMedia.2019025664>
- [9] Siddheshwar, P. G., A. Chan, and U. S. Mahabaleswar. "An Analytical Study of Weakly Nonlinear Dynamics of a Walters' Liquid B around a Flexible Sheet Undergoing Super Linear Stretching." *International Scholarly Research Notices* 2012 (2012). <https://doi.org/10.5402/2012/782369>
- [10] Fang, Tiegang, Ji Zhang, and Shanshan Yao. "A new family of unsteady boundary layers over a stretching surface." *Applied Mathematics and Computation* 217, no. 8 (2010): 3747-3755. <https://doi.org/10.1016/j.amc.2010.09.031>
- [11] Mahabaleswar, U. S., K. R. Nagaraju, P. N. Vinay Kumar, Dumitru Baleanu, and Giulio Lorenzini. "An exact analytical solution of the unsteady magnetohydrodynamics nonlinear dynamics of laminar boundary layer due to an impulsively linear stretching sheet." *Continuum Mechanics and Thermodynamics* 29, no. 2 (2017): 559-567. <https://doi.org/10.1007/s00161-016-0543-9>
- [12] Benos, L. Th, U. S. Mahabaleswar, P. H. Sakanaka, and I. E. Sarris. "Thermal analysis of the unsteady sheet stretching subject to slip and magnetohydrodynamic effects." *Thermal Science and Engineering Progress* 13 (2019): 100367. <https://doi.org/10.1016/j.tsep.2019.100367>
- [13] Anusha, T., Huang-Nan Huang, and U. S. Mahabaleswar. "Two dimensional unsteady stagnation point flow of Casson hybrid nanofluid over a permeable flat surface and heat transfer analysis with radiation." *Journal of the Taiwan Institute of Chemical Engineers* 127 (2021): 79-91. <https://doi.org/10.1016/j.jtice.2021.08.014>
- [14] Choi, S. US, and Jeffrey A. Eastman. *Enhancing thermal conductivity of fluids with nanoparticles*. No. ANL/MSD/CP-84938; CONF-951135-29. Argonne National Lab.(ANL), Argonne, IL (United States), 1995.
- [15] Bhattacharyya, Suvanjan, Plaban Das, Ayan Haldar, and Aritra Rakshit. "Performance Analysis of a Geothermal Air Conditioner Using Nanofluid." In *International Conference on Nano for Energy and Water*, pp. 89-95. Springer, Cham, 2017. [https://doi.org/10.1007/978-3-319-63085-4\\_13](https://doi.org/10.1007/978-3-319-63085-4_13)
- [16] Mahabaleswar, U. S., P. N. Vinay Kumar, and Mikhail Sheremet. "Magnetohydrodynamics flow of a nanofluid driven by a stretching/shrinking sheet with suction." *SpringerPlus* 5, no. 1 (2016): 1-9. <https://doi.org/10.1186/s40064-016-3588-0>

- [17] Benos, Lefteris Th, Nickolas D. Polychronopoulos, Ulavathi S. Mahabaleshwar, Giulio Lorenzini, and Ioannis E. Sarris. "Thermal and flow investigation of MHD natural convection in a nanofluid-saturated porous enclosure: An asymptotic analysis." *Journal of Thermal Analysis and Calorimetry* 143, no. 1 (2021): 751-765. <https://doi.org/10.1007/s10973-019-09165-w>
- [18] Mahabaleshwar, U. S., M. B. Rekha, P. N. Vinay Kumar, F. Selimefendigil, P. H. Sakanaka, G. Lorenzini, and S. N. Ravichandra Nayakar. "Mass transfer characteristics of MHD casson fluid flow past stretching/shrinking sheet." *Journal of Engineering Thermophysics* 29, no. 2 (2020): 285-302. <https://doi.org/10.1134/S1810232820020113>
- [19] Nanjundaswamy, Vinay Kumar Poorigaly, Ulavathi Shettar Mahabaleshwar, Patil Mallikarjun, Mohaddeseh Mousavi Nezhad, and Giulio Lorenzini. "Casson Liquid Flow due to Porous Stretching Sheet with Suction/Injection." In *Defect and Diffusion Forum*, vol. 388, pp. 420-432. Trans Tech Publications Ltd, 2018. <https://doi.org/10.4028/www.scientific.net/DDF.388.420>
- [20] Mukhopadhyay, Swati, Prativa Ranjan De, Krishnendu Bhattacharyya, and G. C. Layek. "Casson fluid flow over an unsteady stretching surface." *Ain Shams Engineering Journal* 4, no. 4 (2013): 933-938. <https://doi.org/10.1016/j.asej.2013.04.004>
- [21] Pramanik, S. "Casson fluid flow and heat transfer past an exponentially porous stretching surface in presence of thermal radiation." *Ain Shams Engineering Journal* 5, no. 1 (2014): 205-212. <https://doi.org/10.1016/j.asej.2013.05.003>
- [22] Fang, Tiegang, and Wei Jing. "Closed-form analytical solutions of flow and heat transfer for an unsteady rear stagnation-point flow." *International Journal of Heat and Mass Transfer* 62 (2013): 55-62. <https://doi.org/10.1016/j.ijheatmasstransfer.2013.02.049>
- [23] Mahabaleshwar, U. S., K. R. Nagaraju, M. N. Nadagoud, R. Bennacer, and Dumitru Baleanu. "An MHD viscous liquid stagnation point flow and heat transfer with thermal radiation and transpiration." *Thermal Science and Engineering Progress* 16 (2020): 100379. <https://doi.org/10.1016/j.tsep.2019.100379>
- [24] Xenos, Michalis A., Eugenia N. Petropoulou, Anastasios Siokis, and U. S. Mahabaleshwar. "Solving the nonlinear boundary layer flow equations with pressure gradient and radiation." *Symmetry* 12, no. 5 (2020): 710. <https://doi.org/10.3390/sym12050710>
- [25] Mahabaleshwar, U. S., K. R. Nagaraju, PN Vinay Kumar, M. N. Nadagouda, R. Bennacer, and M. A. Sheremet. "Effects of Dufour and Soret mechanisms on MHD mixed convective-radiative non-Newtonian liquid flow and heat transfer over a porous sheet." *Thermal Science and Engineering Progress* 16 (2020): 100459. <https://doi.org/10.1016/j.tsep.2019.100459>
- [26] Hiemenz, Karl. "Die Grenzschicht an einem in den gleichformigen Flussigkeitsstrom eingetauchten geraden Kreiszyylinder." *Dinglers Polytech. J.* 326 (1911): 321-324.